

Study on the anti-correlated painting injection scheme for the Rapid Cycling Synchrotron of the China Spallation Neutron Source

Ming-Yang Huang^{a,b,c}, Shouyan Xu^{a,c}, Yuwen An^{a,c}, Jianliang Chen^{a,c},
Liangsheng Huang^{a,c}, Mingtao Li^{a,c}, Yong Li^{a,c}, Zhiping Li^{a,c}, Xiaohan
Lu^{a,c}, Jun Peng^{a,c}, Yue Yuan^{a,c}, Sheng Wang^{a,b,c,1}

^a*Institute of High Energy Physics, Chinese Academy of Sciences, Beijing 100049, China*

^b*University of Chinese Academy of Sciences, Beijing 100049, China*

^c*Spallation Neutron Source Science Center, Dongguan 523808, China*

Abstract

In the rapid cycling synchrotron of the China Spallation Neutron Source, the anti-correlated painting was adopted for the design scheme of the injection system. In the beam commissioning, with the optimization of the anti-correlated painting, the injection beam loss was well controlled and the injection efficiency has exceeded 99%. Combined with other aspects of adjustments, the beam power on the target has reached 50 kW smoothly. In this paper, we have studied the injection optimization in the beam commissioning. Compared to the simulation results of the design scheme, the transverse beam distribution, transverse coupling effect and beam loss of the anti-correlated painting in the beam commissioning were somewhat different. Through the machine studies, we have carefully analyzed these differences and studied their reasons.

Keywords: CSNS, Injection, Painting, Beam commissioning

PACS: 29.25.Dz, 29.27.-a, 29.27.Ac

1. Introduction

The China Spallation Neutron Source (CSNS) is a high power proton accelerator-based facility with the design beam power of 100 kW and repe-

¹Corresponding author email: wangsheng@ihep.ac.cn

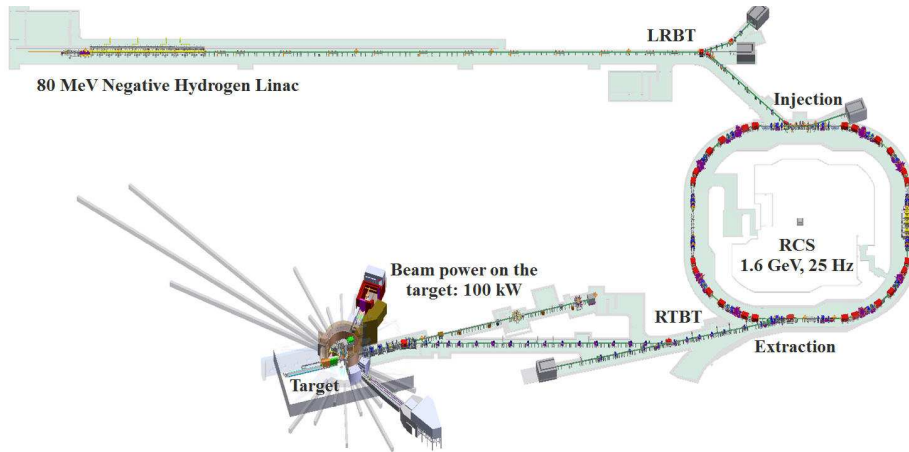


Figure 1: The schematic layout of the CSNS.

tition rate of 25 Hz [1][2]. The schematic layout of the CSNS is shown in Fig. 1. Its accelerator consists of a 1.6 GeV rapid cycling synchrotron (RCS) and an 80 MeV H^- Linac [3]. The RCS accumulates and accelerates an 80 MeV injection beam to the design energy of 1.6 GeV and then extracts the high energy beam to the target. Its lattice has a four-fold structure with four long straight sections for the injection, extraction, RF cavity and beam collimation respectively.

The injection system is the core part of the CSNS accelerator and the injection efficiency is an important factor that determines whether the accelerator can operate safely [4]. The injection process determines the initial state of the circulating beam and has an important influence on the processes of beam accumulation and acceleration. For the injection system, the H^- stripping [5][6][7] is adopted to inject the Linac beam to the RCS with high precision and high efficiency. In order to control the strong space charge effects [8][9][10], which is the main cause of the beam loss, the phase space painting is used [11][12][13] for injecting a small emittance beam from the Linac into the large acceptance of the RCS. The anti-correlated painting scheme was adopted for the injection system [4][14].

The paper is organized as follows. In Sec. 2, the design scheme of the anti-correlated painting is introduced and discussed. In Sec. 3, the injection beam commissioning is studied. The results of the beam commissioning are given and compared to the simulation results. The summary and discussion are given in the last section.

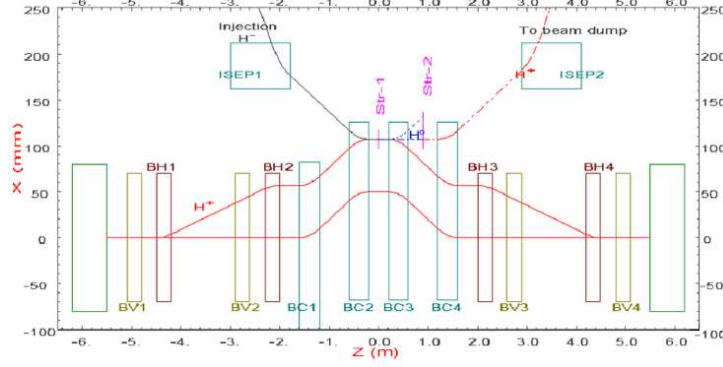


Figure 2: The schematic diagram of the injection system.

2. Design scheme of the anti-correlated painting

In the design stage, by using the codes ORBIT [15] and SIMPSONS [16], the correlated painting and anti-correlated painting of the injection process and acceleration process were simulated [17][18][19]. According to the simulation results, compared to the correlated painting, the transverse coupling effect and beam loss of the anti-correlated painting with the nominal working point (4.86, 4.78) were smaller. Therefore, the anti-correlated painting scheme was adopted.

For the CSNS/RCS, the injection system consists of four bump magnets BC1-BC4 which generates a horizontal chicane bump of 60 mm, four horizontal painting magnets BH1-BH4, four vertical painting magnets BV1-BV4, two septum magnets (ISEP1, ISEP2), a primary stripping foil (Str-1), and a secondary stripping foil (Str-2), as shown in Fig. 2.

In the injection process, the circulating beam moves from the positive maximum to the center in the horizontal plane while it moves from the negative maximum to the center in the vertical plane. The injection point is located in the lower left corner of the main stripping foil to reduce the traversal times of the main stripping foil. Fig. 3 shows the schematic of the RCS acceptance ellipse and injection beam in the injection process.

For the anti-correlated painting, a square-root-type function for the phase-space offset of the injection beam relative to the RCS closed orbit is chosen:

$$X = X_{max} - (X_{max} - X_{min})\sqrt{\frac{t}{T_{inj}}}, \quad X' = 0, \quad (1)$$

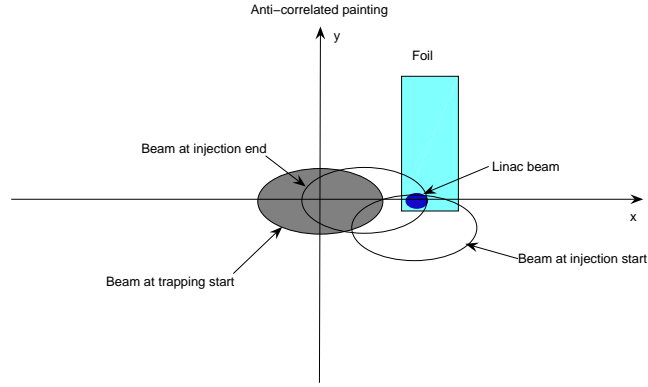


Figure 3: Schematic of the RCS acceptance ellipse and injection beam in the anti-correlated painting process.

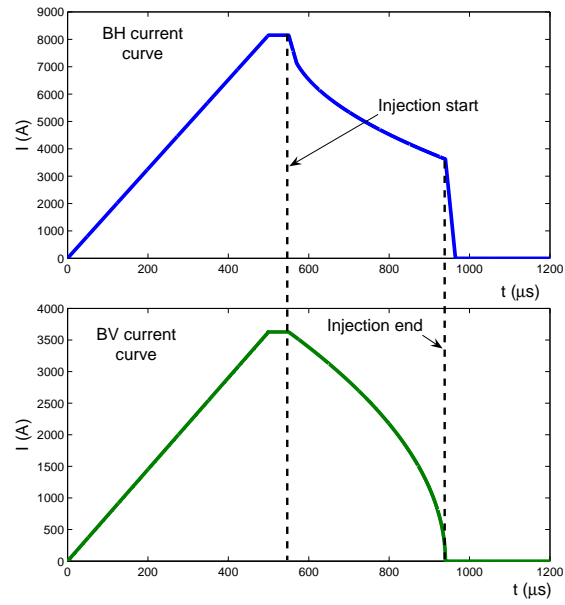


Figure 4: The BH and BV pulse current curves for the anti-correlated painting scheme.

in the horizontal plane and

$$Y = -Y_{max} \times \sqrt{1 - \frac{t}{T_{inj}}}, \quad Y' = 0, \quad (2)$$

in the vertical plane, where $X_{max} - X_{min}$ is the horizontal painting range, Y_{max} is the vertical painting range, T_{inj} is the injection time which is 0.39 ms. Since the injection point of the Linac beam sets at $(X_{max}, 0)$, the maximum horizontal painting emittance depends on $|X_{max} - X_{min}|$ and the maximum vertical painting emittance depends on $|Y_{max}|$. Fig. 4 shows the BH and BV pulse current curves for the anti-correlated painting scheme in which the falling parts of the BH and BV pulse current curves are used for painting.

In order to describe the basic idea of the painting injection in terms of the painting area size in comparison with the machine aperture along the injection bump orbit, the relationship between the emittance of the circulating beam relative to the vacuum chamber center and the machine aperture of the vacuum chamber needs to be studied in detail. Since $D_x \sim 0$ and $D_y \sim 0$ near the injection point, the beam size of the circulating beam can be calculated by

$$\sigma_x^2 = \beta_x \cdot \varepsilon_x, \quad \sigma_y^2 = \beta_y \cdot \varepsilon_y, \quad (3)$$

where ε_x and ε_y are the horizontal and vertical emittances of the circulating beam, β_x and β_y are the Courant-Snyder parameters near the injection point. Supposing the deviation position of the vacuum chamber center relative to circulating beam as (x_0, y_0) , the horizontal and vertical emittances of the circulating beam relative to the vacuum chamber center can be calculated by

$$\varepsilon_{rx} = \frac{[|X - x_0| + |\sigma_x|]^2}{\beta_x}, \quad \varepsilon_{ry} = \frac{[|Y - y_0| + |\sigma_y|]^2}{\beta_y}, \quad (4)$$

where X and Y are the horizontal and vertical painting positions during the injection process. Therefore, supposing the machine aperture radius of the circular vacuum chamber as R , the injection beam loss requires that the whole painting process should meet the following condition:

$$R > \sqrt{\varepsilon_{rx} \cdot \beta_x + \varepsilon_{ry} \cdot \beta_y}. \quad (5)$$

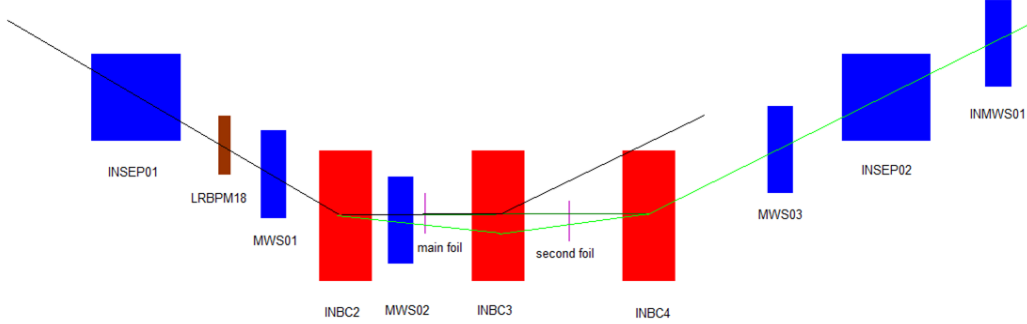


Figure 5: The schematic layout of the I-dump beam line.

3. Beam commissioning

In this section, the results and problems of the beam commissioning for the CSNS injection system would be studied. First of all, the beam parameters between the Linac beam and circulating beam needed to be matched. In order to complete the beam accumulation process as soon as possible, the fixed-point injection method was used in the early stage. The fixed-point injection method means that the relative positions of the injected beam center and circulating beam center remain constant during the injection process. With the increase of injection beam power, the transverse phase space painting was used to reduce the beam loss. The painting ranges and painting curves were optimized and compared to the simulation results of the design scheme. In order to solve the problem of the middle concave of the extraction beam distribution, three aspects of adjustments were carried out. After the above optimizations, the injection beam loss was well controlled and the injection efficiency was over 99%. Combined with other aspects of the beam commissioning, the beam power on the target was over 50 kW and the stable operation was achieved.

3.1. Injection beam parameters matching

In order to measure the injection beam parameters and adjust the injection beam orbit precisely, the I-dump beam line mode was designed [20], as shown in Fig. 5. There are four multi-wire scanners (MWs) on the I-dump beam line. In the beam commissioning, by using two of the four MWs, the phase space coordinates of the Linac beam at the injection point can be measured. By adjusting the injection magnets, the phase space coordinates of the

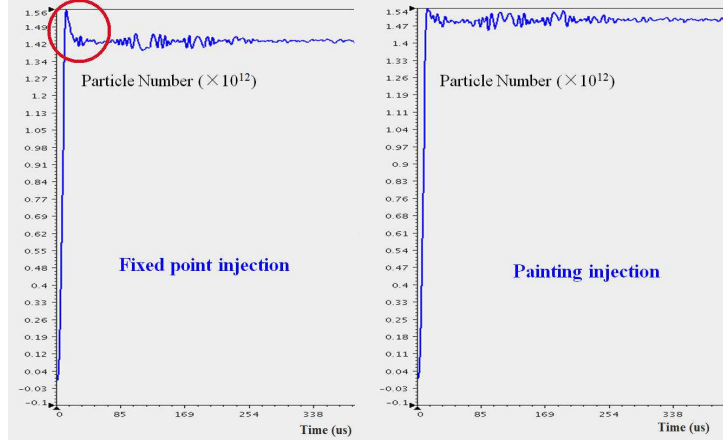


Figure 6: RCS DCCT displays when the fixed-point injection and painting injection were used.

injection beam was calibrated to the reasonable ranges which can basically meet the requirements of the injection beam parameters matching.

A mismatch of phase space coordinates between the injection beam and circulating beam can lead to non-uniform beam distribution and larger emittances as well as additional beam loss. In Ref. [21], a new and more accurate method based on multi-turn injection and Fourier fitting was developed to match the injection orbit. The machine study shows that the mismatch of injection parameters can be well depressed by using this new method.

3.2. A comparative study of the fixed-point injection and painting injection

Since the injection beam power was relatively small in the early stage of the beam commissioning, the fixed-point injection method was selected. However, when the beam power on the target reached 10 kW, there was a sudden beam loss in the injection process no matter the matching between the injection beam and circulating beam, as shown in Fig. 6. By using the transverse phase space painting instead of the fixed-point injection, the sudden beam loss in the injection process was gone. Fig. 6 shows the RCS direct-current current transformer (DCCT) display when the fixed-point injection and painting injection were used. It can be found that, with the transverse phase space painting, the sudden beam loss was gone and the injection efficiency had been improved. The main reason of this phenomenon is that, on the one hand, when the beam density increased in case of the fixed-point injection, the total emittance of the circulating beam would be

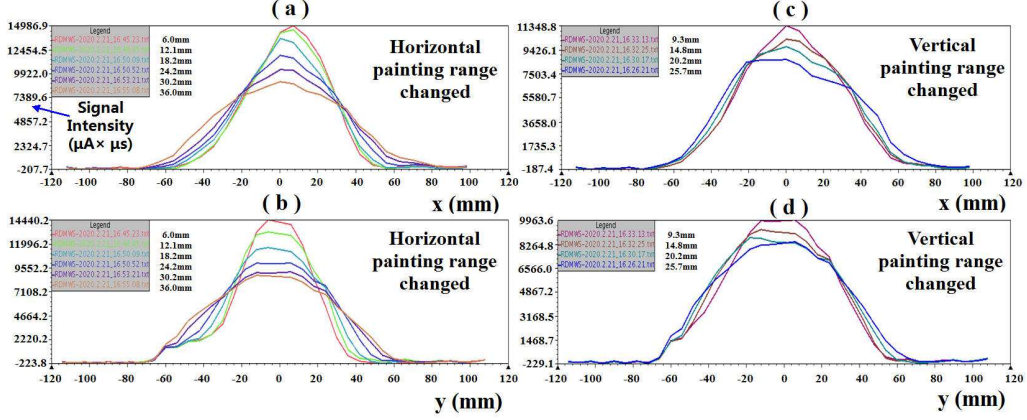


Figure 7: Transverse beam distributions changing with the horizontal and vertical painting ranges when the anti-correlated painting and working point (4.81, 4.87) were used. Sub-graphs (a) and (b): the horizontal painting range was changed when the vertical painting range was fixed to 12 mm; subgraphs (c) and (d): the vertical painting range was changed when the horizontal painting range was fixed to 27 mm.

increased for the strong space charge effects; on the other hand, in the fixed-point injection, to match the injection beam, the center of the circulating beam was bumped to the wall of the vacuum chamber, and the acceptance of injection area was accordingly decreased. In case of the painting injection, the space charge effects would be depressed by painting, and the center of the circulating beam would move to the center of the vacuum chamber during the injection process.

3.3. Study on the painting ranges and transverse coupling effect

According to the simulation results of the design scheme, the optimal horizontal and vertical painting ranges were 33 mm and 26 mm for the anti-correlated painting. In the beam commissioning, in order to measure the transverse beam distribution after painting, a fast extraction scheme was designed by adjusting the extraction timing and extraction mode. When the injection painting completed, the circulating beam was extracted quickly and then measured by a multi-wire scanner which is on the beam transport line from the RCS to the target (RTBT). Therefore, the transverse beam distribution just after painting can be obtained, as shown in Fig. 7. It can be found that the transverse beam sizes increase with the painting ranges. The fact that both of the horizontal and vertical beam sizes increase greatly

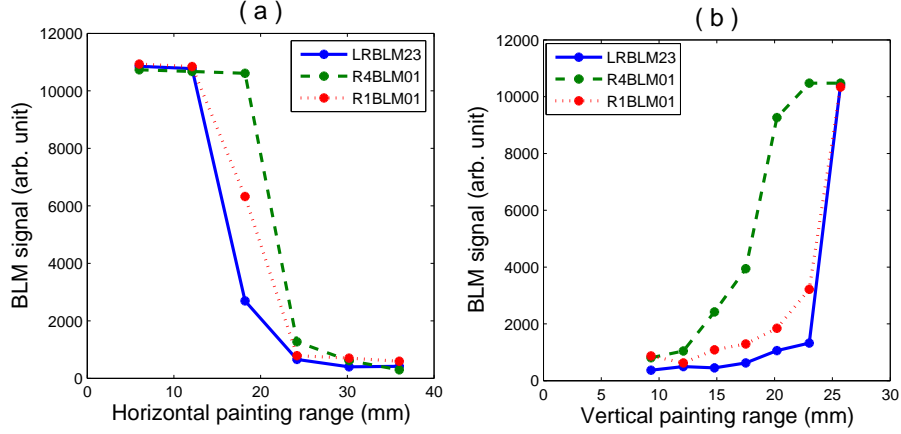


Figure 8: Injection beam loss changing with the horizontal and vertical painting ranges when the anti-correlated painting was used. Subgraph (a): the horizontal painting range was changed when the vertical painting range was fixed to 12 mm; subgraph (b): the vertical painting range was changed when the horizontal painting range was fixed to 27 mm.

with the horizontal painting range suggests that the transverse coupling effect is serious.

By studying the variation of the injection beam loss with the transverse painting ranges, the painting ranges have also been optimized, as shown in Fig. 8. In the figure, all the three beam-loss monitors (LRBLM23, R4BLM01, R1BLM01) are very close to the injection point. LRBLM23 locates on the beam line from the Linac to the RCS (LRBT). R4BLM01 and R1BLM01 locate on either side of the injection point of the RCS. These three beam-loss monitors can basically reflect the injection beam loss. Therefore, it can be found that, when the horizontal painting range is smaller than 27 mm, the injection beam loss begins to grow rapidly. The reason of this phenomenon is that the circulating beam moves from the edge to the center in the horizontal painting process. If the horizontal painting range is too small, the circulating beam will be too close to the edge of the vacuum chamber and resulting in a large amount of beam loss. When the vertical painting range is greater than 12 mm, the injection beam loss begins to increase rapidly. Combining the study of the transverse beam sizes and injection beam loss, the optimal horizontal painting range is 31 mm which is close to the simulation result. The optimal vertical painting range is less than 15 mm which is very different from the simulation result.

According to the previous simulation results, the transverse coupling effect was very small for the anti-correlated painting by using the nominal working point (4.86, 4.78). However, in the beam commissioning, the transverse coupling effect was serious. In order to study the transverse coupling effect, the anti-correlated painting processes for different working points were studied. Fig. 9 shows the transverse beam distributions changing with the horizontal and vertical painting ranges for different working points. It can be found that, with the working point (4.81, 4.87) which is used for the stable operation now, the transverse coupling effect is serious. However, with the working point (4.86, 4.80) which is close to the design values, the transverse coupling effect is smaller. Therefore, different transverse coupling effects caused by different working points result in the great difference between the actual vertical painting range and simulation result.

Although the transverse coupling effect of the working point (4.86, 4.80) is small, the coherent oscillation effect caused by this working point is very large which produces a large amount of beam loss. On the contrary, for the working point (4.81, 4.87), although the transverse coupling effect is a little large, the coherent oscillation effect is very small. The beam loss caused by the combination of these two effects is small and can meet the requirement of the stable operation. Therefore, in the beam commissioning, the transverse coupling effect and coherent oscillation effect should be considered at the same time in choosing the optimal working point.

3.4. *Painting curves optimization*

According to the design scheme of the anti-correlated painting, when the painting curves with a large painting speed in the center and a small painting speed in the edge for both horizontal and vertical directions, as shown in Fig. 4 and Eqs. (1)-(2), the transverse beam distribution was the most uniform and the injection results were the best after painting.

In the beam commissioning, by using the fast extraction scheme, the transverse beam distribution just after painting have be obtained. Fig. 10 shows the transverse beam distributions changing with the horizontal and vertical painting curves. $a = d^2I/dt^2$ is the variation rate of the slope of the painting curve. Combining the mechanical structure of CSNS injection system with Fig. 10, no matter in the horizontal or vertical plane, when the painting curve with a small painting speed in the center and a large painting speed in the edge, the transverse beam sizes after painting are small.

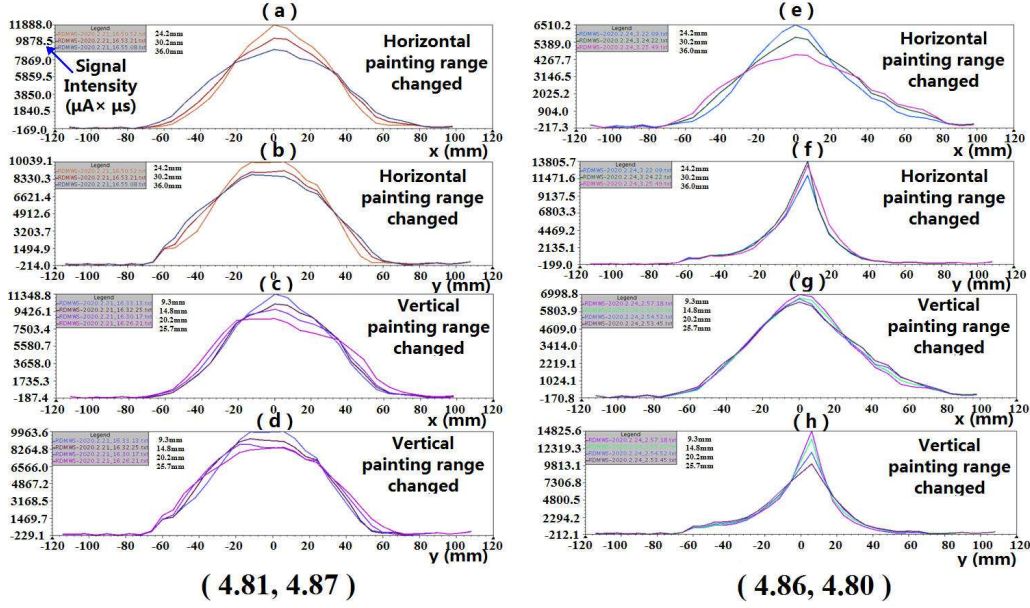


Figure 9: Transverse beam distributions changing with the horizontal and vertical painting ranges for different working points when the anti-correlated painting was used. Subgraphs (a), (b), (e) and (f): the horizontal painting range was changed when the vertical painting range was fixed to 12 mm; subgraphs (c), (d), (g) and (h): the vertical painting range was changed when the horizontal painting range was fixed to 27 mm.

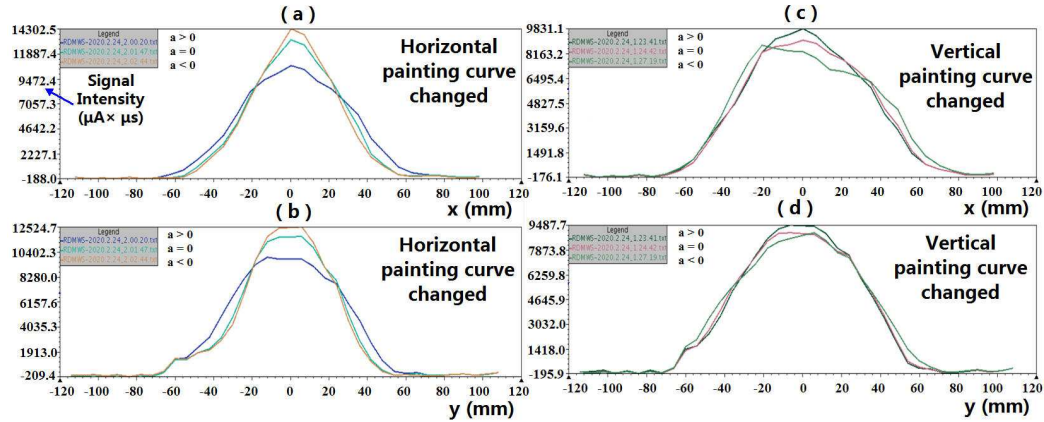


Figure 10: Transverse beam distributions changing with the horizontal and vertical painting curves when the anti-correlated painting was used. Subgraphs (a) and (b): the horizontal painting curve was changed when the vertical painting curve was fixed to $a > 0$; subgraphs (c) and (d): the vertical painting curve was changed when the horizontal painting curve was fixed to $a > 0$.

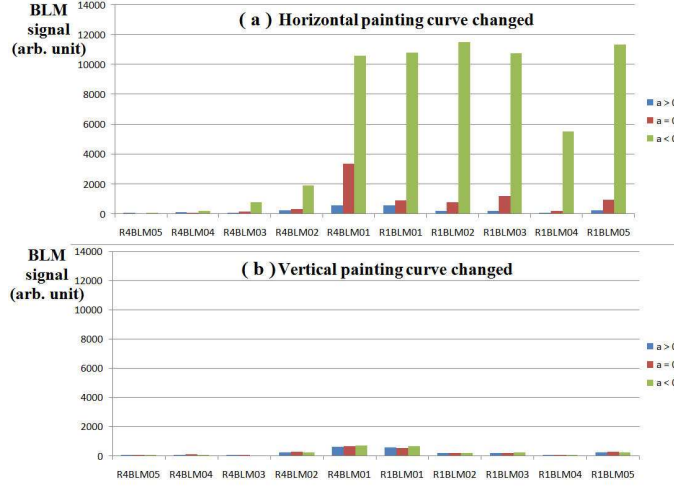


Figure 11: Injection beam loss changing with the horizontal and vertical painting curves when the anti-correlated painting was used. Subgraph (a): the horizontal painting curve was changed when the vertical painting curve was fixed to $a > 0$; subgraph (b): the vertical painting curve was changed when the horizontal painting curve was fixed to $a > 0$.

By studying the variation of the injection beam loss with the painting curves, the painting curves have also be optimized. Fig. 11 shows the injection beam loss changing with the horizontal and vertical painting curves. In the figure, all the ten beam-loss monitors (R4BLM05, R4BLM04, R4BLM03, R4BLM02, R4BLM01, R1BLM01, R1BLM02, R1BLM03, R1BLM04, R1BLM05) locate in the injection region. It can be seen that, when the horizontal painting curve with a small painting speed in the center and a large painting speed in the edge, the injection beam loss is very large. The main reason of this phenomenon is that the circulating beam is very close to the wall of the vacuum chamber of the injection system at initial moment of horizontal painting. If the painting speed is too slow, it is easy to touch the wall of the vacuum chamber and result in a large amount of injection beam loss in the horizontal plane. Combining Figs. 10 and 11, the optimal horizontal painting curve has a large painting speed in the center and a small painting speed in the edge. The optimal vertical painting curve has a small painting speed in the center and a large painting speed in the edge. Therefore, the optimal horizontal painting curve is consistent with the simulation result while the optimal vertical painting curve differs greatly from the simulation result. Fig. 12 shows the difference between the actual optimal vertical painting

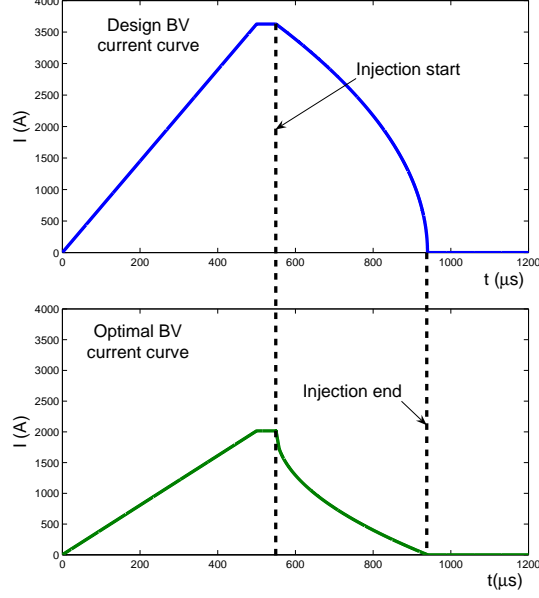


Figure 12: The design and optimal BV pulse current curves for the anti-correlated painting scheme.

curve and the design vertical painting curve for the anti-painting scheme.

3.5. Optimization of the extraction beam distribution

Although the hollow painting method was not used, the extraction beam distribution appeared a middle concave in the horizontal plane which is very different from the simulation result. There may be three reasons for this phenomenon: (1) the injection timing was not accurate enough; (2) the matching between the injection beam and circulating beam was not accurate enough; (3) the rising edge of the injection beam was of poor quality.

In the beam commissioning, the injection beam timing was precisely adjusted, the injection beam and circulating beam were accurately matched, and the rising edge of the injection beam was cut off by using the chopper. Fig. 13 shows the time structure of the injection beam. The upper figure shows the original injection beam and the lower figure shows the injection beam after cutting off the rising edge. After these three aspects of optimizations, the extraction beam distribution in the horizontal plane was no

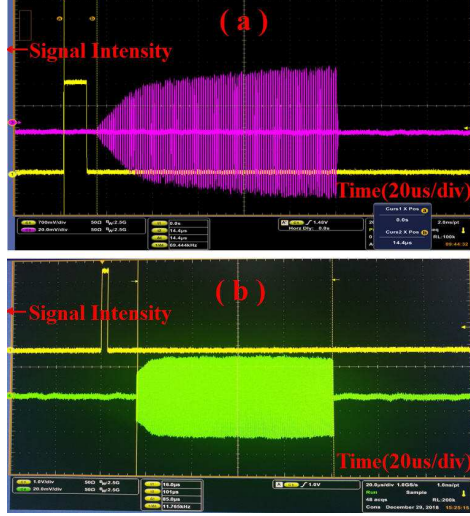


Figure 13: The time structure of the injection beam. Subgraph (a): before cutting off the rising edge; subgraph (b): after cutting off the rising edge.

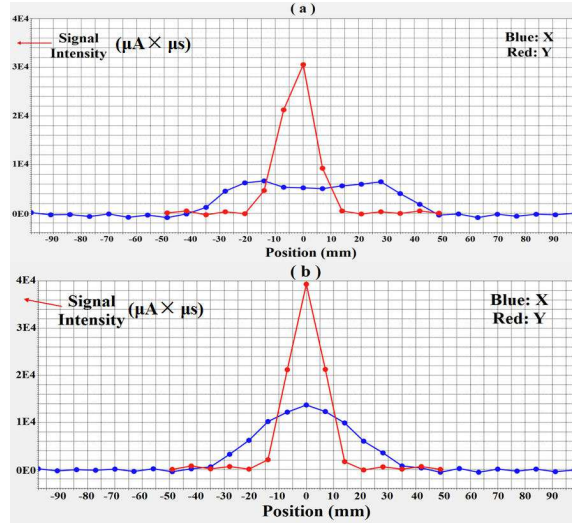


Figure 14: Beam distribution on the target. Subgraph (a): before the injection optimization; subgraph (b): after the injection optimization.

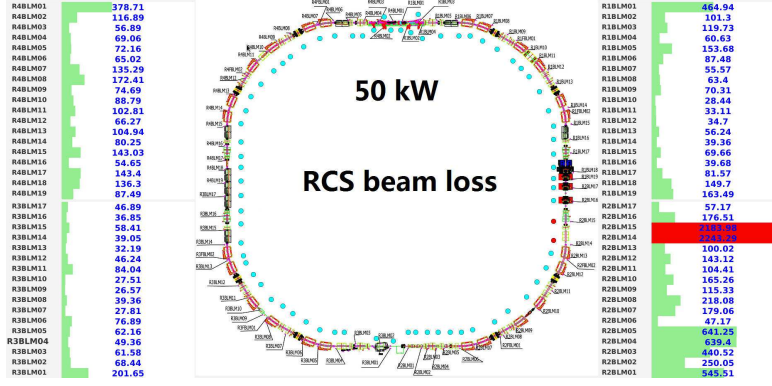


Figure 15: RCS beam loss of 50 kW beam power on the target when the anti-correlated painting was used.

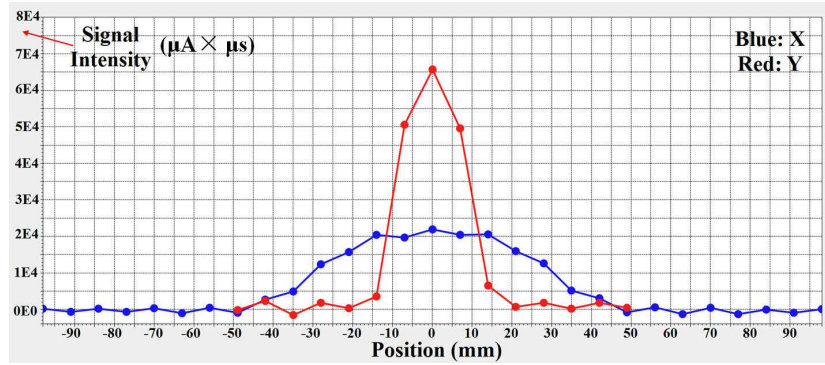


Figure 16: Beam distribution on the target of 50 kW beam power when the anti-correlated painting was used.

longer concave in the middle, as shown in Fig. 14. It is consistent with the simulation result which is close to the Gaussian distribution.

3.6. Achieve 50 kW beam power on the target

After the injection beam parameters matching, stripping foil optimization, phase space painting optimization, extraction beam optimization and injection beam loss regulation, the injection beam loss was well controlled and the injection efficiency was over 99%. Combined with other aspects of the beam commissioning, the beam power on the target has exceeded 50 kW and achieved the stable operation. Fig. 15 and Fig. 16 show the RCS beam loss and beam distribution on the target of 50 kW beam power. Fig. 17

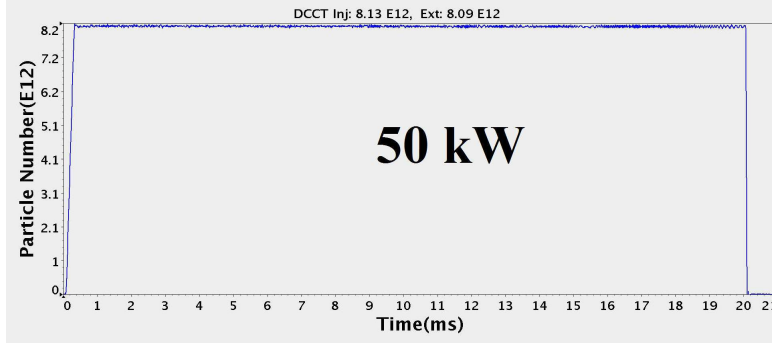


Figure 17: RCS DCCT display of 50 kW beam power on the target when the anti-correlated painting was used.

shows the RCS DCCT display of 50 kW beam power on the target when the anti-correlated painting was used. It can be seen from these figures that: both the injection efficiency and RCS transmission efficiency are very high; the beam distribution and beam loss have met the requirements of the stable operation.

4. Summary and discussion

In this paper, firstly, the design scheme of the anti-correlated painting for CSNS/RCS was introduced and studied. Then, the beam commissioning of the injection system was studied. Compared to the simulation results of the design scheme, the transverse beam distribution, transverse coupling effect and beam loss of the actual anti-correlated painting were somewhat different. By using the machine studies, we have analyzed these differences and studied their reasons. After the optimization, the beam power on the target has exceeded 50 kW and achieved the stable operation. In order to further improve the beam power on the target, the further comparative study between the correlated and anti-correlated painting schemes should be conducted in the future.

Acknowledgments

The authors would like to thank H.C. Liu, Y.L. Zhang, P. Zhu, Z.H. Xu and other CSNS colleagues for helpful discussions. M.Y. Huang also would like to thank Yoshiro Irie of KEK for helpful discussions. This work was

supported by National Natural Science Foundation of China (Project Nos. U1832210 and 12075134).

References

References

- [1] S. Wang et al., Introduction to the overall physics design of CSNS accelerators, Chin. Phys. C, 33 (S2) (2009) 1-3.
- [2] J. Wei, Synchrotrons and accumulators for high-intensity proton beams, Rev. Mod. Phys., 75 (4) (2003) 1383-1432.
- [3] J. Wei et al., China Spallation Neutron Source - an overview of application prospects, Chin. Phys. C, 33 (11) (2009) 1033-1042.
- [4] M.Y. Huang, S. Wang, J. Qiu, N. Wang, S.Y. Xu, Effects of injection beam parameters and foil scattering for CSNS/RCS, Chin. Phys. C, 37 (6) (2013) 067001.
- [5] T. Kawakubo, Analysis and measurement of beam dynamics in H^- charge-exchange injection, Nucl. Instrum. Methods Phys. Res. A, 265 (1988) 351-363.
- [6] A.H. Mohagheghi et al., Interaction of relativistic H^- ions with thin foils, Phys. Rev. A, 43 (1991) 1345-1365.
- [7] A.I. Drozhdin, I.L. Rakhno, S.I. Striganov, L.G. Vorobiev, Modeling multiturn stripping injection and foil heating for high intensity proton drivers, Phys. Rev. ST Accel. Beams, 15 (2012) 011002.
- [8] J.A. Holmes, V.V. Danilov, J.D. Galambos, D. Jeon, D.K. Olsen, Space charge dynamics in high intensity rings, Phys. Rev. ST Accel. Beams, 2 (1999) 114202.
- [9] S. Cousineau, S.Y. Lee, J.A. Holmes, V. Danilov, A. Fedotov, Space charge induced resonance excitation in high intensity rings, Phys. Rev. ST Accel. Beams, 6 (2003) 034205.
- [10] S.Y. Xu, S. Wang, Study on space charge effects of the CSNS/RCS, Chin. Phys. C, 35 (12) (2011) 1152-1158.

- [11] J. Wei et al., Injection choice for Spallation Neutron Source ring, in: Proceedings of the Particle Accelerator Conference, Chicago, United States, 2001, pp. 2560-2562.
- [12] J. Beebe-Wang, Y.Y. Lee, D. Raparia, J. Wei, Transverse phase space painting for SNS accumulator ring injection, in: Proceedings of the Particle Accelerator Conference, New York, United States, 1999, pp. 1743-1745.
- [13] J. Beebe-Wang, Y.Y. Lee, D. Raparia, J. Wei, Beam properties in the SNS accumulator ring due to transverse phase space painting, in: Proceedings of the European Particle Accelerator Conference, Vienna, Austria, 2000, pp. 1465-1467.
- [14] J.Y. Tang, J. Qiu, S. Wang, J. Wei, Physics design and study of the BSNS RCS injection system, Chin. Phys. C, 30 (12) (2006) 1184-1189.
- [15] J. Gabambos, J. Holmes, D. Olsen, ORBIT user's manual V1.0, SNS-ORNL-AP Tech. Note 11, 1999.
- [16] S. Machida, The Simpsons program user's reference Manual V1.0, July, 1992
- [17] J. Qiu, J.Y. Tang, S. Wang, J. Wei, Studies of transverse phase space painting for the CSNS RCS injection, Chin. Phys. C, 31 (10) (2007) 942-946.
- [18] T. Wei, S. Wang, J. Qiu, J.Y. Tang, Q. Qin, Beam-loss driven injection optimization for CSNS/RCS, Chin. Phys. C, 34 (2) (2010) 218-223.
- [19] S.Y. Xu, S.X. Fang, S. Wang, The study of the space charge effects for RCS/CSNS, in: Proceedings of HB2010, Morschach, Switzerland, 2010, pp. 420-424.
- [20] M.Y. Huang et al., Measurement of the injection beam parameters by the multi-wire scanner for CSNS, in: Proceedings of the 9th International Particle Accelerator Conference (IPAC2018), Vancouver, BC, Canada, 2018, pp. 1014-1016.
- [21] X.H. Lu, M.Y. Huang, S. Wang, Injection orbit matching for a rapid cycling synchrotron, Phys.Rev. Accel. Beams, 21 (2018) 062802.